was based on the absence of detectable isotope exchange during the induction period over a temperature range of 1200–1800 K. Our barrier of about 70 kcal/mol is significantly above their lower bound. The energy of the hexagonal transition state is clearly below the dissociation limit of an individual hydrogen molecule. This can, in principle, provide a molecular pathway for isotope exchange distinct from an atomic pathway. (As discussed in the Introduction, it is clear that a bimolecular pathway has not been observed in shock tubes.)

Knowledge of potential energy differences alone is often not sufficient to completely characterize the course of a chemical process. Internal energy distribution and content, as well as the dynamical behavior of a system often determines much of the chemistry observed. If a termolecular process were to take place via a six-centered transition state as investigated here, dynamical studies would also require some knowledge of the tunneling probability for the hydrogen atoms. This, however, is beyond the scope of this investigation. In this light we should mention that there has been one quasi-classical trajectory study[33] of the H_6 termolecular reaction, with the reactants being a van der Waals bound dimer and a hydrogen molecule.

$$A_2B_2 + C_2 \rightarrow AB + AC + BC \qquad (5)$$

The potential surface used was constructed to mimic a model reaction with a barrier height of 69 kcal/mol. If only translational energy is provided, this study predicted a dynamic barrier of 90 kcal/mol. However, vibrational energy did significantly enhance the termolecular process. Unfortunately, this study had too few trajectories to provide statistical significance. In a related experiment, Herman[7] studied the reverse reaction to (2), where HD was excited to $v = 5$ ($\Delta E = 47$ kcal/mol) by using a cw intracavity dye laser, but no D_2 production was observed. This laser experiment was not sensitive enough, however, to detect products from a six-center reaction. In another experiment Bauer and co-workers[34] excited room-temperature H_2 or D_2 to $v = 1$ in a bulb using stimulated Raman scattering. They did observe HD product accounting for it by $v - v$ collisionally pumped H_2 ($v \geq 3$) and a bimolecular process. Vibrational enhancement coupled with a termolecular process could also account for this yield although the barrier used in the kinetic model calculations was somewhat low.[14] It is also possible that HD was produced in the stimulated Raman bulb experiments from catalysis on the walls or, as suggested by Herman, from H atoms produced by collisions. All of the results seem to be consistent with the failure to observe a bimolecular mechanism for H/D exchange in H_2/D_2 mixtures under any of the experimental conditions employed thus far.

V. Conclusions

We have reported here an investigation of the transition state for the termolecular reaction involving H_2/D_2 exchange to produce HD. This reaction has been of long-standing interest since historically there has been a sharp divergence between the best experiments and the most detailed theoretical calculations. The calculations presented here suggest that a termolecular process is energetically and possibly even dynamically feasible. The full CI calibration results have shown that with present computational methods we can provide energies within the accepted chemical accuracy of ±1 kcal/mol. The calculations were done with a large one-particle basis, and the level of correlation accounts for most of the molecular correlation in this six-electron system. Detailed studies of other termolecular processes will be forthcoming.

Acknowledgment. P.R.T. acknowledges the support of NASA Ames Research Center on Grant NCC2-371. A.K. thanks NASA Ames for access to the computational facilities. Part of this work was performed with a grant of computer time from the NAS Facility.

Registry No. H_2, 1333-74-0.

(33) NoorBatcha, I.; Thareja, S.; Sathyamurthy, N. *J. Phys. Chem.* **1987**, *91*, 2171.

(34) Bauer, S. H.; Lederman, D. M.; Resler, E. L., Jr.; Fisher, E. R. *Int. J. Chem. Kinet.* **1973**, *5*, 93.

Single-Crystal EPR Spectrum of the Phosphido-Bridged Radical $Fe_2(CO)_7(\mu\text{-}PPh_2)$

Paul J. Krusic,*,† R. Thomas Baker,† Joseph C. Calabrese,† John R. Morton,‡ Keith F. Preston,*,‡ and Yvon Le Page‡

Contribution from the Central Research and Development Department, E. I. du Pont de Nemours and Company,⊥ Wilmington, Delaware 19898, and the Division of Chemistry, National Research Council of Canada, Ottawa, Ontario, Canada K1A OR9. *Received May 24, 1988*

Abstract: The EPR spectrum of the 33e phosphido-bridged radical $Fe_2(CO)_7(\mu\text{-}PPh_2)$ has been measured in single crystals of the diamagnetic host $FeCo(CO)_7(\mu\text{-}PPh_2)$ at 77 K. **g** and hyperfine interaction tensors for a ^{31}P and two distinct ^{13}C nuclei were determined for the radical in an orthogonal axis system of the triclinic host whose crystal structure was established by X-ray diffractrometry (space group $P\bar{1}$; $a = 9.057$ (2) Å; $b = 13.001$ (3) Å; $c = 8.713$ (3) Å; $\alpha = 105.25$ (2)°; $\beta = 95.21$ (2)°; $\gamma = 84.32$ (2)°; $Z = 2$). The values of the tensor components and their directions in the crystal structure clearly show that the radical is isostructural with the host molecule. Unpaired spin density is essentially confined to the pentacoordinated iron nucleus and two of its carbonyl ligands. These ligands and the two iron nuclei form the equatorial plane (xy) of a distorted trigonal-bipyramidal structure in which the unpaired electron occupies an Fe d_{xy} orbital. Extended Hückel molecular orbital calculations are in excellent agreement with the experimental findings.

In the past 10 years or so considerable progress has been made in the structural determination of precariously stable organometallic molecules. EPR spectroscopy has played no small role in this endeavor, although much still remains to be accomplished. The EPR spectrometer used in conjunction with single-crystal samples offers an unequalled probe for the determination of the atomic orbital composition of the ground electronic wave function of a free radical. As a bonus, the technique supplies information on the disposition of electronically excited states through the measurement of the **g** matrix. While the structures of a number of mononuclear transition-metal radicals have now been established,[1] less progress has been made for polynuclear species.

† E. I. du Pont de Nemours and Company.
‡ National Research Council of Canada.
⊥ NRCC No. 29792, du Pont Contribution No. 4348.

0002-7863/89/1511-1262$01.50/0

Table I. Summary of X-ray Diffraction Data

complex	$FeCo(CO)_7(\mu\text{-}PPh_2)$
formula	$C_{19}H_{10}CoFeO_7P$
fw	496.04
a, Å	9.057 (2)
b, Å	13.001 (3)
c, Å	8.713 (3)
α, deg	105.25 (2)
β, deg	95.21 (2)
γ, deg	84.32 (2)
v, Å^3	982.7
Z	2
ρ_{calcd}, g cm^{-3}	1.676
space group	$P\bar{1}$ (No. 2)
cryst dimens, mm	0.38 × 0.26 × 0.36
temp, °C	−100
radiation	Mo Kα
μ, cm^{-1}	16.98
data collection	ω–2θ
max 2θ, deg	55.0
scan speed, deg/min	2.00–8.90
scan width, deg	1.20ω
total no. of observations	4851
no. of unique data, $I > 3.0\sigma(I)$	3748
final no. of variables	262
final max shift/error	0.07
max residual density, e/Å^3	0.36
R^a	0.023
$R_w{}^b$	0.029

$^a \sum||F_o| - |F_c||/\sum|F_o|$. $^b [\sum w(|F_o| - |F_c|)^2/\sum wF_o^2]^{1/2}$.

Structural studies of such species have considerable bearing on our understanding of catalytic processes, and EPR investigations could make an important contribution in this area.

The extent of delocalization of the unpaired electron in polynuclear metal radicals is of great interest, particularly in cases where two transition-metal centers are connected by a bridging ligand. A notable instance[2,3] is the isolable phosphido-bridged radical $Fe_2(CO)_7(\mu\text{-}PPh_2)$, in which the unpaired electron is believed to be essentially confined to one iron nucleus of an asymmetric structure. The unusual structure of this species and its conformational non-rigidity led us to investigate its EPR spectrum in a single-crystal matrix of the diamagnetic analogue $FeCo(CO)_7(\mu\text{-}PPh_2)$. The latter was thought to be a particularly good matrix since the two complexes appear to be isostructural judging by the striking similarity of their IR spectra.[2,3]

Experimental Section

(a) Preparation. The 33e radical $Fe_2(CO)_7(\mu\text{-}PPh_2)$ and the diamagnetic host $FeCo(CO)_7(\mu\text{-}PPh_2)$ were prepared according to literature methods.[2,4] Recrystallization from cold *n*-hexane generated black, irregular crystals of $FeCo(CO)_7(\mu\text{-}PPh_2)$ which proved suitable for X-ray crystallography. A portion of the host was doped with radical before recrystallization in order to obtain crystals for examination by EPR spectroscopy: Sufficient dry, oxygen-free *n*-hexane was added under vacuum to dissolve a mixture of the two solids containing ~0.1% free radical, and the resulting solution was kept in a sealed tube at 10 °C until crystals formed. Single crystals were then selected with the aid of a polarizing microscope.

(b) Crystallography. X-ray diffraction data were collected at −100 °C on a Syntex R3 diffractometer with use of graphite-filtered Mo radiation. The data were reduced in the usual fashion for Lorentz and polarization effects, and the solution and refinement of the structure were carried out on a VAX cluster system with a local program set. Heavy-atom positions were obtained via automated Patterson analysis and used to phase the reflections for the remaining light atoms through the usual combination of structure factor, Fourier synthesis, and least-squares refinement. The refinement was performed with full-matrix least-squares, with anisotropic thermal parameters for all non-hydrogen atoms; anomalous dispersion terms[5] for Fe, Co, and P were included as well as idealized coordinates for the hydrogen coordinates as fixed-atom contributors. A summary of the diffraction data is presented in Table I; final positional and thermal parameters for atoms appear in Table II, and selected bond distances and angles are listed in Table III. Tables of general temperature factors (Table VI) and structure factor listings (Table VII) and a figure with the complete atom numbering system are available as Supplementary Material.

Table II. Atomic Coordinates (×10000) and Temperature Factors for $FeCo(CO)_7(\mu\text{-}PPh_2)$

atom	x	y	z	$B_{iso}{}^a$
Co(1)	1519.3 (3)	1866.1 (2)	10307.0 (3)	1.5 (1)
Fe(1)	2778.6 (3)	938.7 (2)	7601.9 (3)	1.3 (1)
P(1)	1378.3 (5)	2503.6 (4)	8260.2 (5)	1.4 (1)
O(1)	5320 (2)	2139 (1)	9244 (2)	2.4 (1)
O(2)	144 (2)	−318 (1)	6638 (2)	2.5 (1)
O(3)	4412 (2)	−1033 (1)	8123 (2)	2.5 (1)
O(4)	3509 (2)	938 (1)	4404 (2)	3.5 (1)
O(5)	−1544 (2)	2140 (1)	11200 (2)	3.0 (1)
O(6)	3267 (2)	3343 (1)	12759 (2)	3.6 (1)
O(7)	2446 (2)	−125 (1)	11199 (2)	2.5 (1)
C(1)	4316 (2)	1693 (1)	8648 (2)	1.8 (1)
C(2)	1120 (2)	198 (1)	7028 (2)	1.8 (1)
C(3)	3783 (2)	−278 (1)	7924 (2)	1.8 (1)
C(4)	3205 (2)	934 (2)	5638 (2)	2.1 (1)
C(5)	−368 (2)	2013 (2)	10783 (2)	2.0 (1)
C(6)	2622 (2)	2778 (2)	11752 (2)	2.2 (1)
C(7)	2072 (2)	651 (2)	10849 (2)	1.8 (1)
C(11)	2327 (2)	3690 (1)	8335 (2)	1.7 (1)
C(12)	2112 (2)	4595 (2)	9594 (2)	2.1 (1)
C(13)	2805 (3)	5513 (2)	9663 (3)	2.7 (1)
C(14)	3719 (2)	5539 (2)	8494 (3)	2.7 (1)
C(15)	3945 (2)	4649 (2)	7246 (3)	2.6 (1)
C(16)	3253 (2)	3727 (2)	7158 (2)	2.3 (1)
C(21)	−321 (2)	2671 (1)	7023 (2)	1.8 (1)
C(22)	−449 (3)	3389 (2)	6067 (3)	3.0 (1)
C(23)	−1732 (3)	3483 (2)	5098 (3)	3.8 (1)
C(24)	−2892 (2)	2874 (2)	5062 (3)	3.2 (1)
C(25)	−2787 (2)	2167 (2)	6009 (3)	2.6 (1)
C(26)	−1515 (2)	2067 (2)	6996 (2)	2.1 (1)
H(12)	1481	4586	10415	3.0
H(13)	2655	6137	10534	3.0
H(14)	4191	6178	8547	3.0
H(15)	4589	4665	6436	3.0
H(16)	3411	3109	6281	3.0
H(22)	356	3817	6088	3.0
H(23)	−1800	3977	4435	3.0
H(24)	−3776	2938	4387	3.0
H(25)	−3592	1731	5979	3.0
H(26)	−1455	1573	7659	3.0

^{a} Anisotropically refined atoms are given in the form of the isotropic equivalent thermal parameter defined as $4/3[a^2B_{11} + b^2B_{22} + c^2B_{33} + ab(\cos\gamma)B_{12} + ac(\cos\beta)B_{13} + bc(\cos\alpha)B_{23}]$.

(c) EPR Spectroscopy. Single crystals of radical doped into $FeCo(CO)_7(\mu\text{-}PPh_2)$ were oriented on a Nonius diffractometer according to the known structural parameters of the host. Once oriented, the crystals were sealed with epoxy glue into the ends of 4 mm quartz tubes such that each of the standard set[6] of orthogonal axes X,Y,Z in turn was aligned along the tube axis. A pointer was attached to the tube to indicate the direction of one of these axes in the perpendicular plane. The tube was placed in a dewar of liquid nitrogen which was inserted into the rectangular cavity of a Varian E12 spectrometer. EPR spectra were recorded and measured with standard accessories as a function of angle between the tube pointer and the dc magnetic field. In some instances, a radical-doped single crystal was mounted on a Teflon two-circle goniometer[7] and transferred directly to the cavity of the EPR spectrometer. The goniometer settings required to explore a crystal plane were generated by a computer program.[7]

(d) Molecular Orbital Calculations. MO calculations were carried out through the du Pont implementation of the extended Hückel method[8]

(1) Symons, M. C. R.; Morton, J. R.; Preston, K. F. *ACS Symp. Ser.* **1987**, *333*, 169.
(2) Baker, R. T.; Krusic, P. J.; Calabrese, J. C.; Roe, D. C. *Organometallics* **1986**, *5*, 1506.
(3) Baker, R. T.; Calabrese, J. C.; Krusic, P. J.; Therien, M. J.; Trogler, W. C. *J. Am. Chem. Soc.*, in press.
(4) Benson, B. C.; Jackson, R.; Joshi, K. K.; Thompson, D. T. *J. Chem. Soc., Chem. Commun.* **1968**, 1506.
(5) *International Tables for X-ray Crystallography*; Kynoch Press: Birmingham, UK, 1974; Vol. IV, Tables 2.2B and 2.31.
(6) Rollett, J. S. *Computing Methods in Crystallography*, Pergamon: Oxford, 1965; Chapter 3.
(7) Morton, J. R.; Preston, K. F. *J. Magn. Reson.* **1983**, *52*, 457.
(8) Pensak, D. A.; McKinney, R. J. *Inorg. Chem.* **1979**, *18*, 3407. McKinney, R. J.; Pensak, D. A. *Ibid.* **1979**, *18*, 3413.

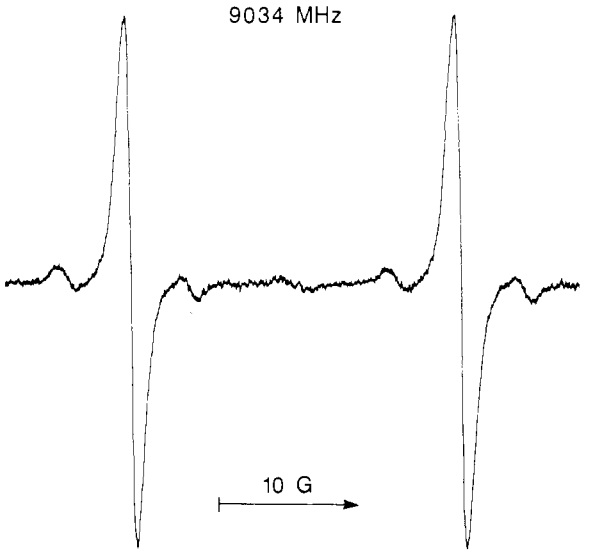

Figure 1. First-derivative EPR spectrum of $Fe_2(CO)_7(\mu\text{-}PPh_2)$ in a single crystal of $FeCo(CO)_7(\mu\text{-}PPh_2)$ at 77 K for H_0 near X. Satellite absorptions associated with each component of the ^{31}P doublet are due to hyperfine interactions with ^{13}C nuclei present in natural abundance.

Table III. Selected Bond Distances (Å) and Angles (deg) for $FeCo(CO)_7(\mu\text{-}PPh_2)$

	a. Distances		
Co(1)-Fe(1)	2.6516 (10)	P(1)-C(11)	1.823 (2)
Co(1)-P(1)	2.1445 (8)	P(1)-C(21)	1.826 (2)
Co(1)-C(5)	1.776 (2)	O(1)-C(1)	1.136 (2)
Co(1)-C(6)	1.792 (2)	O(2)-C(2)	1.136 (2)
Co(1)-C(7)	1.778 (2)	O(3)-C(3)	1.131 (2)
Fe(1)-P(1)	2.2548 (8)	O(4)-C(4)	1.135 (2)
Fe(1)-C(1)	1.817 (2)	O(5)-C(5)	1.138 (2)
Fe(1)-C(2)	1.824 (2)	O(6)-C(6)	1.141 (2)
Fe(1)-C(3)	1.820 (2)	O(7)-C(7)	1.141 (2)
Fe(1)-C(4)	1.787 (2)		
	b. Angles		
Fe(1)-Co(1)-P(1)	54.86 (3)	C(1)-Fe(1)-C(2)	166.41 (7)
Fe(1)-Co(1)-C(5)	131.02 (6)	C(1)-Fe(1)-C(3)	89.33 (8)
Fe(1)-Co(1)-C(6)	115.23 (7)	C(1)-Fe(1)-C(4)	96.45 (9)
Fe(1)-Co(1)-C(7)	85.71 (6)	C(2)-Fe(1)-C(3)	88.17 (8)
P(1)-Co(1)-C(5)	101.80 (6)	C(2)-Fe(1)-C(4)	97.12 (9)
P(1)-Co(1)-C(6)	103.01 (7)	C(3)-Fe(1)-C(4)	103.51 (9)
P(1)-Co(1)-C(7)	139.78 (5)	Co(1)-P(1)-Fe(1)	74.08 (3)
C(5)-Co(1)-C(6)	111.7 (1)	Co(1)-P(1)-C(11)	119.98 (6)
C(5)-Co(1)-C(7)	98.76 (9)	Co(1)-P(1)-C(21)	125.00 (7)
C(6)-Co(1)-C(7)	100.87 (9)	Fe(1)-P(1)-C(11)	115.36 (6)
Co(1)-Fe(1)-P(1)	51.05 (2)	Fe(1)-P(1)-C(21)	118.11 (6)
Co(1)-Fe(1)-C(1)	81.67 (6)	C(11)-P(1)-C(21)	102.96 (9)
Co(1)-Fe(1)-C(2)	86.11 (6)	Co(1)-C(5)-O(5)	175.0 (2)
Co(1)-Fe(1)-C(3)	105.26 (6)	Co(1)-C(6)-O(6)	174.8 (2)
Co(1)-Fe(1)-C(4)	151.14 (7)	Co(1)-C(7)-O(7)	179.0 (4)
P(1)-Fe(1)-C(1)	85.72 (6)	Fe(1)-C(1)-O(1)	176.7 (2)
P(1)-Fe(1)-C(2)	91.23 (6)	Fe(1)-C(2)-O(2)	175.8 (2)
P(1)-Fe(1)-C(3)	156.27 (6)	Fe(1)-C(3)-O(3)	180 (1)
P(1)-Fe(1)-C(4)	100.11 (7)	Fe(1)-C(4)-O(4)	178.3 (2)

with the inclusion of the two-body repulsions introduced by Anderson.[9] Parameters were taken from the literature.[8]

Results

For an arbitrary direction of the crystal with respect to the dc magnetic field, the EPR spectrum (Figure 1) consisted of a doublet of ~30 G splitting. This splitting is attributed to hyperfine coupling of a single unpaired electron with a ^{31}P nucleus ($I = {}^1/_2$) in the free-radical impurity. The observation of a single magnetic site for all directions conforms with the structure of the host $FeCo(CO)_7(\mu\text{-}PPh_2)$ crystal which belongs to the triclinic system.

(9) Anderson, A. B. *J. Chem. Phys.* **1975**, *62*, 1187. See also: Anderson, A. B. *J. Am. Chem. Soc.* **1978**, *100*, 1153 and references therein.

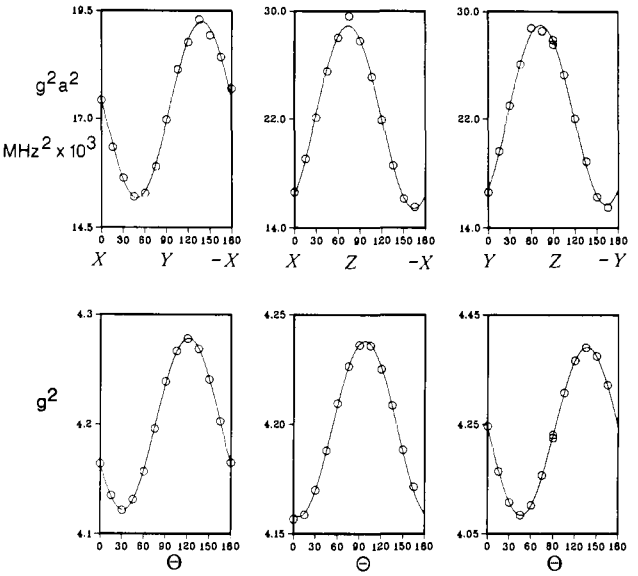

Figure 2. Plots of g^2 and g^2a^2 (10^3 MHz^2) against angle for the three orthogonal crystal planes of $FeCo(CO)_7(\mu\text{-}PPh_2)$. Least-squares best-fit sine curves have been drawn through the experimental points (circles).

Table IV. The $\mathbf{g}^2$ and Hyperfine Tensors $\mathbf{ga}^2\mathbf{g}$ (MHz^2) for the Radical $Fe_2(CO)_7(\mu\text{-}PPh_2)$ in a $FeCo(CO)_7(\mu\text{-}PPh_2)$ Crystal. The Principal Values of **g** and Hyperfine Interactions in MHz and Their Direction Cosines in the *XYZ* Axis System

	tensor			principal values and direction cos of **g**, $\mathbf{a}_{31}$, and $\mathbf{a}_{13}$		
	X	*Y*	*Z*	*x*	*y*	*z*
				2.0132	2.0454	2.0973
	4.1615	−0.0693	−0.0102	0.4740	−0.8612	0.1834
$\mathbf{g}^2$	−0.0693	4.2405	−0.1538	0.6564	0.2067	−0.7255
	−0.0102	−0.1538	4.2332	0.5869	0.4643	0.6633
				55.8	66.7	84.6 MHz
	17022	−2020	3565	0.6133	0.7575	0.2238
$\mathbf{ga}_{31}{}^2\mathbf{g}$	−2020	16984	3754	0.6979	−0.6524	0.2954
P	3565	3754	27740	−0.3698	0.0250	0.9288
				18.1	24.2	32.9 MHz
	2448	307	57	0.1834	0.9722	0.1459
$\mathbf{ga}_{13}{}^2\mathbf{g}$	307	2843	1449	−0.7255	0.0337	0.6874
C_1	57	1449	3009	0.6633	−0.2319	0.7115
				18.1	19.1	30.3 MHz
	3671	24	−591	0.1834	0.1710	0.9680
$\mathbf{ga}_{13}{}^2\mathbf{g}$	24	1457	12	−0.7255	0.6880	0.0159
C_2	−591	12	1617	0.6633	0.7053	−0.2503

The spectrum was detectable throughout the range 4–300 K, although individual lines were twice as broad at 300 K as they were at 100 K and below. Accordingly, this single-crystal study was undertaken at 77 K ($\Delta H \cong 1.3$ G p–p).

First-order g and ^{31}P hyperfine coupling were calculated from the spectra as a function of angle within a chosen plane. For each crystal plane, the values of g^2 and of g^2a^2 were plotted (Figure 2) against angle and best-fit matrix elements for $\mathbf{g}^2$ and **gaag** were determined from least-squares computer fits to expressions of the type

$$g^2 = g_{xx}{}^2 \cos^2\theta + g_{yy}{}^2 \sin^2\theta + g_{xy}{}^2 \sin 2\theta$$

The matrix of $\mathbf{g}^2$ was diagonalized to generate its principal values and directions, and the **g** matrix was assembled in the crystal (X,Y,Z) axis system. The inverse of **g** was used to pre- and post-multiply the $\mathbf{ga}^2\mathbf{g}$ matrix to give the $\mathbf{a}^2$ matrix in the crystal-axis system.[7] This was then diagonalized to generate the principal values and directions of the phosphorus hyperfine interaction. Table IV summarizes the experimental data in matrix form.

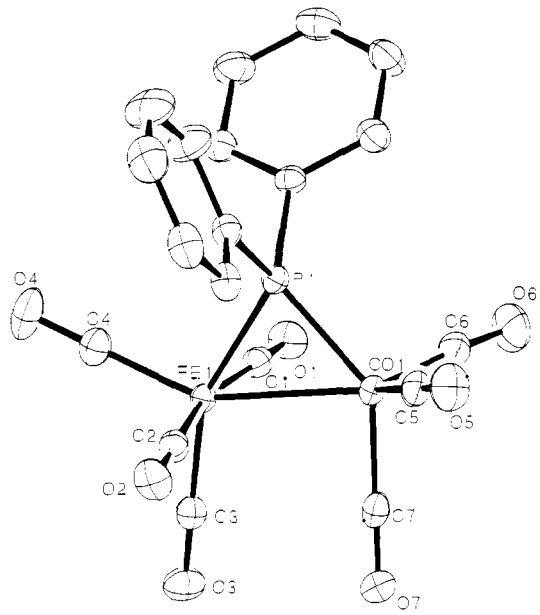

Figure 3. Structure of the host molecule $FeCo(CO)_7(\mu\text{-}PPh_2)$.

Weak satellite lines associated with each component of the ^{31}P hyperfine doublet were ascribed to further interactions of the unpaired electron with two distinct carbon nuclei (^{13}C, $I = {}^1/_2$, natural abundance $\cong$ 1%). Initial measurements suggested that resolution of the ^{13}C structure would be optimal in a plane perpendicular to the direction of g_{max}. Accordingly, a single crystal doped with the free radical enriched in ^{13}C was mounted on the two-circle goniometer and the appropriate plane explored. The squares of the ^{13}C hyperfine couplings were measured as a function of angle in that plane; for the two remaining principal planes of $\mathbf{g}^2$ it was noticed that the turning points for $\mathbf{a}_{13}{}^2$ occurred along the principal directions of $\mathbf{g}^2$. Matrices of $\mathbf{g}^2\mathbf{a}_{13}{}^2$ were rotated into the crystal X,Y,Z basis and diagonalized to yield principal values and directions in that basis (Table IV).

For certain directions very close to that of g_{max}, additional weak satellite lines were detected outside the ^{13}C resonances of an intensity appropriate for a single ^{57}Fe nucleus in natural abundance (^{57}Fe, $I = {}^1/_2$, 2.2% natural abundance). The ^{57}Fe coupling near g_{max} was approximately 13 G. Unfortunately, the weak iron satellites were obscured by the ^{13}C resonances for all other directions, so that it did not prove possible to assemble a complete hyperfine matrix for ^{57}Fe.

Discussion

A consideration of the experimental observations enables us to conclude that the EPR spectrum in crystals of $FeCo(CO)_7(\mu\text{-}PPh_2)$ is associated with the substitutional impurity $Fe_2(CO)_7(\mu\text{-}PPh_2)$. Dealing first with the principal values of $\mathbf{g}$ and ^{31}P hyperfine interaction, we note that these are very close to those already reported for the free radical in frozen 3-methylpentane.[2] Furthermore, the size of the isotropic ^{31}P hyperfine interaction is typical of α-phosphorus couplings in metal-centered radicals.[10-12] Closer inspection of the principal directions of the $\mathbf{g}$ and ^{13}C tensors will show that the free radical is, in fact, isostructural with the host molecule, as already suspected from an earlier study.[2]

The structure of the host molecule as deduced from the crystallographic measurements is shown in Figure 3, and certain bond lengths and directions are given in Tables III and V. The phosphido group bridges a six-coordinate iron and a five-coordinate cobalt atom (Figure 3). The coordination of atoms C_1 to C_4 and

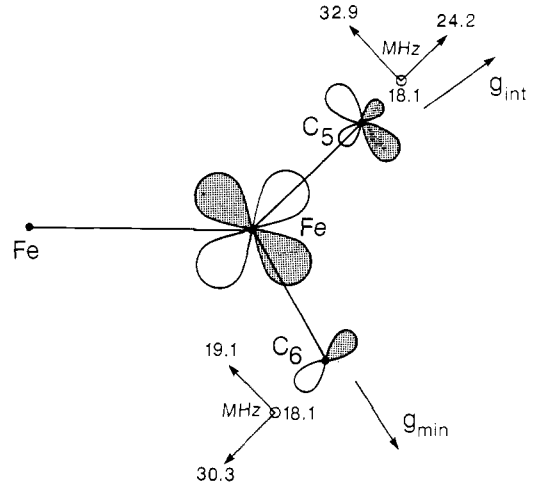

Figure 4. A possible SOMO for the radical, consistent with the experimental data, showing the constituent atomic orbital angular distributions in the equatorial plane.

Table V. Certain Bond Angles, Lengths, and Direction Cosines in the Orthogonal Axis System of the $FeCo(CO)_7(\mu\text{-}PPh_2)$ Crystal

		direction cosines		
bond	length (nm)	X	Y	Z
Fe–Co	0.2652	−0.4271	0.4052	0.8083
P–Co	0.2144	0.0591	−0.3682	0.9279
C_5–Co	0.1776	0.9558	−0.0288	−0.2927
C_6–Co	0.1791	−0.5535	−0.6819	−0.4781
C_7–Co	0.1778	−0.2795	0.8352	−0.4737
perpendicular to plane				
Fe–Co–P		0.8238	0.5430	0.1630
C_5–Co–C_6		−0.1999	0.6661	−0.7186

P about the iron atom is roughly square pyramidal with C_4 as apex. While we were unable to find any close correlation between principal directions of either $\mathbf{g}$ or $\mathbf{a}_{31}$ with bond directions radiating from the Fe atom, a correspondence was immediately apparent at the Co end of the molecule: g_{max} lay only 4.7° from the perpendicular to the C_5CoC_6 plane; g_{min} lay 7.9° from the CoC_6 bond; and g_{int} lay 15.2° from the CoC_5 bond. The Fe, Co, C_5, and C_6 atoms are very nearly coplanar (Figure 3) and CoC_7 lies some 17.7° away from the perpendicular to their plane. This plane may be regarded as the equatorial plane of a trigonal-bipyramidal arrangement of the ligands about the Co atom. In this description the P and C_7 atoms are axial ligands showing significant distortions from their normal (i.e., perpendicular) positions. We were unable to find a correlation between the principal directions of the ^{31}P tensor and directions of bonds or perpendiculars to planes in the host crystal. Moreover, the phosphorus and $\mathbf{g}$ tensors were distinctly non-parallel. These facts clearly indicate that the free radical adopts the low symmetry of the host molecule with the unpaired spin confined to the pentacoordinated nucleus. Measurements made of the ^{13}C and ^{57}Fe tensors support this conclusion.

Only two ^{13}C hyperfine interactions were detected for the radical. These have very similar principal values (Table IV) and their smallest components both lie along the direction of g_{max}. The largest components of the ^{13}C tensors lie in the CoC_5C_6 plane approximately 90° apart (Figure 4), and one of them lies within 4° of the CoC_5 bond direction. While carbon atoms 5 and 6 are clearly implicated in the semioccupied molecular orbital (SOMO) of the free radical, we cannot unambiguously assign the ^{13}C tensors to the individual nuclei. One possibility for the SOMO consistent with the data of Table IV and with our extended Hückel calculations (see below) is illustrated in Figure 4. The absolute signs of the hyperfine tensor components are not known, of course, but the two most likely sign combinations for ^{13}C are as follows: (1) all components positive and (2) positive sign for the largest component and negative for the others, as in (−18.1, −24.2, 32.9 MHz), for example. Realistic decompositions of these choices

(10) McCall, J. M.; Morton, J. R.; Preston, K. F. *J. Magn. Reson.* **1985**, *64*, 414.
(11) Kidd, D. R.; Cheng, C. P.; Brown, T. L. *J. Am. Chem. Soc.* **1978**, *100*, 4103.
(12) Baker, P. K.; Connelly, N. G.; Jones, B. M. R.; Maher, J. P.; Somers, K. R. *J. Chem. Soc., Dalton Trans.* **1980**, 579.

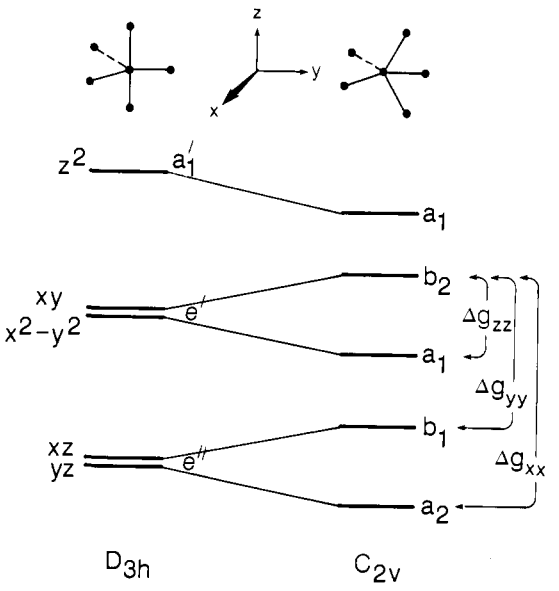

Figure 5. Effects of lowering of symmetry from D_{3h} to C_{2v} on the atomic d levels of a trigonal bipyramid.

for ^{13}C tensors into isotropic and axial components lying in the CoC_5C_6 plane are

$$\begin{aligned} C_5&: \ 25.1 + (-4.9, -4.9, 9.8) + (-2.1, 4.2, -2.1)\ \text{MHz} \\ C_6&: \ 22.5 + (-4.1, -4.1, 8.2) + (-0.3, 0.6, -0.3)\ \text{MHz} \end{aligned} \quad (1)$$

$$\begin{aligned} C_5&: \ -3.1 + (-19.0, -19.0, 38.0) + (4.0, -2.0, -2.0)\ \text{MHz} \\ C_6&: \ -2.3 + (-16.5, -16.5, 33.0) + (0.6, -0.3, -0.3)\ \text{MHz} \end{aligned} \quad (2)$$

When converted into unpaired-spin populations with published one-electron parameters,[13] the tensors (1) suggest 2s contributions to the SOMO of 0.6% from both carbons and in-plane 2p contributions of 7% and 5%, respectively, from C_5 and C_6. The alternative choice (2) suggests 2s contributions of −0.2% from both carbons and in-plane 2p contributions of 20% and 16% respectively from C_5 and C_6. Since the latter spin populations correspond much more closely to those computed (see below) in Hückel calculations, sign choice (2) is most likely correct.

The ^{31}P hyperfine tensor (Table IV) is almost isotropic, so that there can be little doubt that the signs of the components are all the same. Conversion to spin populations[13] leads to only 0.5% in P(3s) and 3% in P(3p), values consistent with the Hückel calculations (see below) that predict essentially zero direct participation of phosphorus orbitals in the SOMO.

The d-level splitting pattern for an undistorted trigonal bipyramid is well-known and is shown in Figure 5. The spin-bearing Fe nucleus in $Fe_2(CO)_7(\mu\text{-}PPh_2)$ is formally Fe(I) and d^7. In the D_{3h} symmetry of an undistorted trigonal bipyramid, the seventh electron would be expected to occupy one of the degenerate e' ($x^2 - y^2$, xy) 3d levels,[14] and this should lead to a Jahn–Teller distortion. In fact, the bridged radical has a "built-in" distortion that lowers the symmetry and splits the e' pair. The expected splitting of the d levels for a trigonal-bipyramidal geometry subject to a C_{2v} distortion, for example, is shown in Figure 5. Strictly speaking, $FeCo(CO)_7(\mu\text{-}Ph_2)$ possesses no symmetry elements (Figure 3) because of twisting induced by the bulky phenyl groups. However, the diamagnetic analogue $FeCo(CO)_7(\mu\text{-}P(CH_3)_2)$ has a plane of symmetry[15] containing the phosphorus and the two metal atoms. Accordingly, in order to simplify the calculations and visualize the make-up of the SOMO, we chose the symmetry and atomic coordinates of the latter diamagnetic analogue in our extended Hückel molecular orbital calculations for the model radical $Fe_2(CO)_7(\mu\text{-}PH_2)$. (PH distances were taken to be 1.46 Å.) The results of these calculations are in excellent qualitative

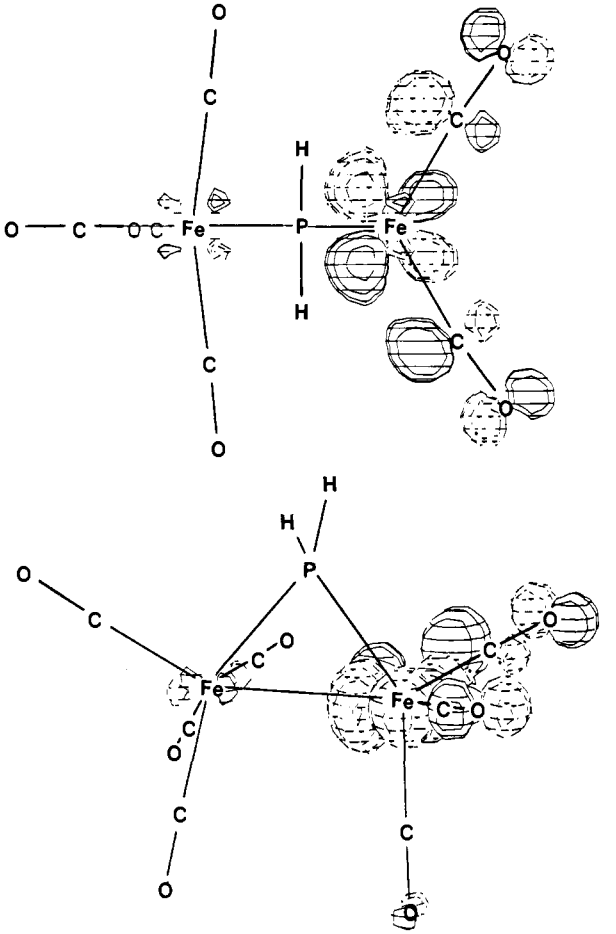

Figure 6. Contour plots from two points of view of the singly occupied molecular orbital of $Fe_2(CO)_7(\mu\text{-}PH_2)$ calculated by the extended Hückel method.

accord with the experimental findings as can be seen from Figure 6, which shows two views of the singly occupied molecular orbital. The unpaired electron is essentially restricted to the five-coordinate iron (43.8%) and the two equatorial CO ligands (42.8%). Other atoms make negligible contributions to the SOMO (6.4% axial CO, 1.1% PH_2, and 5.9% from the remaining atoms). Spin density on the five-coordinate iron is almost entirely located in d_{xy} with a very minor component in p_y, and it is essentially restricted to p_x and p_y atomic orbitals for the equatorial CO ligands. The emergence of ^{57}Fe satellite resonances for directions close to g_{max} conforms with the d_{xy} character of the SOMO: z is the anticipated direction of maximum absolute metal hyperfine interaction, and a 13 G coupling is close to the value predicted from one-electron parameters[13] for ^{57}Fe and the core-polarization term.[16]

In order to check our simplified procedure of retaining a plane of symmetry in the extended Hückel calculations, computations were also carried out for $Fe_2(CO)_7(\mu\text{-}PH_2)$ with the coordinates of the diamagnetic host $FeCo(CO)_7(\mu\text{-}PPh_2)$. The results are quite similar to those presented above for the more symmetric structure, except that the SOMO is now contaminated with minor contributions from other d orbitals of the five-coordinate iron atom.

In the absence of symmetry elements of any kind in the radical, group-theoretical arguments cannot be used to predict g shifts. The orbital schemes of Figure 5 are appropriate to the higher symmetry situation encountered[12] in $Fe(CO)_3L_2^+$ and strictly do not apply in this instance. However, the similarity in **g** tensors for the two cases shows that the C_{2v} scheme to the right of Figure 5 is a fair approximation to the situation at the spin-bearing Fe in $Fe_2(CO)_7(\mu\text{-}PPh_2)$. The C_{2v} group designations no longer apply, of course, and intermixing of the levels in the lower symmetry

(13) Morton, J. R.; Preston, K. F. *J. Magn. Reson.* **1978**, *30*, 577.
(14) Rossi, A. R.; Hoffman, R. *Inorg. Chem.* **1975**, *14*, 365.
(15) Keller, E.; Vahrenkamp, H. *Chem. Ber.* **1977**, *110*, 430.
(16) Symons, M. C. R. *Chemical and Biochemical Aspects of Electron-Spin Resonance Spectroscopy*; Wiley: New York, 1978; Chapter 12.

is possible. A large positive g shift is anticipated for the z direction (g_{max}), since the spin–orbital interaction l_z connects the $x^2 - y^2$, xy levels that were the components of the degenerate e' pair in D_{3h} (Figure 5). The fact that the g shifts along x and y are also positive shows that the empty z^2 orbital is more remote than the filled pair of levels of e'' origin. In the absence of true symmetry elements, the principal directions of **g** will tend to coincide with bond directions or with "approximate" symmetry elements of the radical. In the present example, the C_5CoC_6 plane is clearly a local symmetry element at the spin-bearing end of the radical that determines the direction of g_{max}. With spin density essentially confined to the Fe and equatorial carbons, it is not at all surprising to find that the remaining principal directions are along the metal–carbon bonds. Had the molecule retained the higher symmetry of the $FeCo(CO)_7(\mu\text{-}P(CH_3)_2)$ molecule, one of the *smaller g* values would have *necessarily* fallen perpendicular to the FeCoP symmetry plane, of course. The lowering of symmetry caused by twisting of the phenyl groups thus induces a dramatic reorientation of g_{int} and g_{min}.

Comparison of the isotropic ^{13}C couplings measured in this study with those determined[2] at −80 °C in liquid pentane reveals a discrepancy. The liquid-phase spectrum shows a ^{13}C hyperfine manifold indicative of 5 equivalent carbon nuclei in the radical with hyperfine interactions of 5.9 G. Clearly, the molecule undergoes a rapid fluxional motion at −80 °C, and it has been suggested[2] that this causes interchange of carbons 1, 2, 4, 5, and 6 via a CO-bridged intermediate. In the fast exchange limit, the solution ^{13}C hyperfine interaction should then be the average of the couplings for these carbons in the static molecule, i.e., $(a_1 + a_2 + a_4 + a_5 + a_6)/5$. Since there are no observable ^{13}C satellite lines for carbons 1, 2, and 4, a_1, a_2, and a_4 cannot be much larger than the line width of ca. 1.3 G. Thus, with $(a_5 + a_6)$ being 17 G, the expected hyperfine splitting for the five rapidly interchanging carbons should be no more than 4.2 G, which is smaller than the observed 5.9 G. A plausible explanation for this discrepancy is that the structure of the radical in the crystalline lattice of its diamagnetic host is not exactly the same as the equilibrium structure in solution, that is, the vibrationally averaged structure at the minima of the potential function governing the exchange process. Since the ^{13}C hyperfine interactions for carbons 5 and 6, in particular, are bound to be structure-dependent, their solution values in the slow exchange limit may well be somewhat different from those in the crystalline state.

Although we have been unable to measure the hyperfine interaction tensors of either metal nucleus in the radical, the correlations between principal directions of **g** and $\mathbf{a}_{13}$ with bond directions at *one end* of the molecule establish beyond any doubt that the unpaired spin is localized on one Fe nucleus. This inference was also drawn from the earlier liquid-phase studies. The asymmetrical structure is somewhat surprising in view of the structures of other binuclear carbonyl radicals, where CO bridging is more important.[17-19] In this case, the CO-bridged species is evidently not isolable and corresponds to a maximum of the potential function that governs the facile intramolecular exchange of the five CO ligands.

Finally, we note a close similarity between the **g** tensor components of $Fe_2(CO)_7(\mu\text{-}PPh_2)$ and those of acyltetracarbonyliron radicals[20] and $Fe(CO)_3L_2^+$ radicals,[12] where L is a substituted phosphine or arsine. In the latter case, the similarity extends to the isotropic ^{31}P hyperfine couplings. In all three types of radical, the experimental evidence points to a trigonal-bipyramidal geometry at the spin-bearing Fe nucleus and occupation of one of the pair of e' (xy, $x^2 - y^2$) orbitals by the unpaired electron. Infrared spectroscopic evidence for the liquid phase at room temperature suggests,[12,21] in fact, that the $Fe(CO)_3L_2^+$ radicals are strictly D_{3h} with $^2E'$ ground states. It is therefore most surprising that those radicals have been detected in solution by EPR spectroscopy, since Jahn–Teller radicals are normally not detectable under such conditions. We note, however, that in the frozen state, the radicals have the *non-axial* **g** tensor[12] expected of a Jahn–Teller distorted state.

Acknowledgment. We thank Dr. David L. Thorn for useful discussions and Steven A. Hill for assistance with synthesis. We also thank the referees for reminding us of the analogous $Fe(CO)_3L_2^+$ radicals and suggesting further discussion of principal directions of **g**.

Registry No. $Fe_2(CO)_7(\mu\text{-}PPh_2)$, 102211-00-7; $Fe_2(CO)_7(\mu\text{-}PPh_2)$, 22852-98-8.

Supplementary Material Available: Tables of anisotropic thermal parameters together with a thermal ellipsoid diagram and labeling scheme for the host crystal $FeCo(CO)_7(\mu\text{-}PPh_2)$ (2 pages); listing of structure factors (3 pages). Ordering information is given on any current masthead page.

(17) Lionel, T.; Morton, J. R.; Preston, K. F. *Inorg. Chem.* **1983**, *22*, 145.
(18) Fairhurst, S. A.; Morton, J. R.; Preston, K. F. *Organometallics* **1983**, *2*, 1869.
(19) Krusic, P. J. *J. Am. Chem. Soc.* **1981**, *103*, 2131.
(20) Krusic, P. J.; Cote, W. J.; Grand, A. *J. Am. Chem. Soc.* **1984**, *106*, 4642.
(21) Therien, M. J.; Trogler, W. C. *J. Am. Chem. Soc.* **1986**, *108*, 3697.